AMERICAN SCIENTIFIC PUBLISHERS

Science of Advanced Materials
Vol. 4, pp. 727–733, 2012
(www.aspbs.com/sam)

ARTICLE

Effect of Annealing Temperature on the Performances and Electrochemical Properties of TiO_2 Dye-Sensitized Solar Cells

Junting Xi[1,2,†], Naji Al Dahoudi[2,3,†], Qifeng Zhang[2], Yueming Sun[1,*], and Guozhong Cao[2,*]

[1]*School of Chemistry and Chemical Engineering, Southeast University, Nanjing, Jiangsu 211189, China*
[2]*Department of Materials Science and Engineering, University of Washington, Seattle, WA 98195, USA*
[3]*Physics Department, Al Azhar University-Gaza, P.O.Box 1277, Gaza, Palestine*

ABSTRACT

The influences of thermal annealing on the microstructure, dye-adsorption, surface area, electrical properties and power conversion efficiency of well-crystallized TiO_2 photoelectrodes of dye-sensitized solar cells have been systematically investigated. Although the heat treatment of TiO_2 photoelectrodes at higher temperatures was found to result in an enhanced electron transport, it was accompanied with a reduced specific surface area and less adsorbed dye molecules. A power conversion efficiency of $5.1 \pm 0.2\%$ was obtained with a negligible deviation for the samples heat-treated at temperatures ranging from 350 °C to 600 °C.

KEYWORDS: Dye-Sensitized Solar Cells, Annealing Temperature, Morphology, Surface Area, Impedance Spectroscopy.

1. INTRODUCTION

Dye-sensitized solar cells (DSCs),[1–3] albeit less efficient in power conversion than solar cells made from Si or other semiconducting materials,[4–6] appear as an alternative to produce electricity at low cost, environmental benign, and less energy intensive with continuous rising of oil prices and the pollution concerns, particularly after the Fukushima nuclear plant catastrophe. The energy conversion process in DSCs is composed of injection of electrons from the photo-excited dye molecules into the conduction band of mesoporous TiO_2 photoanode deposited on transparent conducting oxide (TCO) electrode. The oxidized dye molecules are regenerated by the electrons in electrolyte which is simultaneously reduced at the counter electrode.[1,7] The kinetic processes of DSCs depend on many parameters, which in many cases are complicated and related to each others. The existence of many interfaces between TCO, TiO_2, dye molecule, electrolyte and the counter electrode is obviously complex because of several reactions that affect the efficient operation of the device.[8–11] The processes which affect the performance of such devices include the injection and transport of electrons, dye regeneration, electron recombination with the oxidized dye and/or the redox species in electrolyte. Changing any component in the DSCs such as photoanode materials, dye molecules, counter electrode, and electrolyte, would impact the power conversion efficiency. TiO_2 is the most effective and most used photoanode material; any change in its crystalline structure,[12] microstructure,[13,14] and surface chemistry[15] would affect the device performance. Thermal annealing of TiO_2 film is one of the factors explored to optimize the output of the device. Currently TiO_2 nanoparticle photoelectrodes for DSCs are annealed typically at 450 °C in air.[16,17] Thermal annealing effects on the microstructure and dynamics of electron transport and recombination in TiO_2 and ZnO based DSCs, have been investigated partially during the last few years.[18–25] The electron diffusion coefficient and life time increase with the annealing temperature, resulting in more efficient electron transport within the photoelectrode.[19,25] However, the internal surface area of the nanoparticle films decreases simultaneously with enhancing the annealing temperature which affects the dye molecule adsorption as well as the light harvesting.[21] It seems that heat treatment at high temperature is required to sinter the nanoparticle network to promise fast electron transport, induce electrical contact between nanoparticles and TCO, and get rid of the organic compounds initially present; however, annealing at a moderate or low temperature is also needed to retain large specific surface area for dye loading and the large pores for mass transport of the

*Authors to whom correspondence should be addressed.
Emails: sun@seu.edu.cn, gzcao@u.washington.edu
†These two authors contributed equally to this work.
Received: 17 December 2011
Accepted: 7 January 2012

redox shuttle.[26, 27] Moreover, the high annealing temperature would also result in a reduced electrical conductivity of the charge collecting electrode. For some applications, flexible plastic substrates may be used, which cannot withstand temperatures higher than 200 °C, and also highly transparent conductive ITO coated glass substrate is not adequate to be used at temperatures above 350 °C.[28]

Competition between enhanced electron transport and reduced surface area in nanoparticle photoelectrodes is the main bottleneck for developing higher power conversion efficiency. In this work, these two parallel effects as well as performances of DSCs were systematically investigated by varying the annealing temperature of the TiO_2 nanoparticles film from 300 °C to 600 °C. The TiO_2 nanoparticles used in this work were already well-crystallized, which will be helpful to better understand the relationship between film quality and solar cell performance by changing the annealing temperature, without affecting the crystal properties of nanoparticles.

2. EXPERIMENTAL DETAILS

2.1. Fabrication of TiO_2 Nanoparticle Films

Nanoparticles of TiO_2 used in this work were obtained by hydrothermally treating TiO_2 sol, as previously described.[29] For dye-sensitized solar cell application, TiO_2 nanoparticle films with thickness ~15 μm were coated on FTO glass substrates by doctor-blading a paste of 25 wt% powder in organic binder mainly based on α-terpineol and ethyl cellulose. The films were preheated at 150 °C for 30 min and further annealed at various temperatures, 300 °C, 350 °C, 400 °C, 450 °C, 500 °C, 550 °C and 600 °C, for 1 h at the same heating rate of 10 °C/min. The as-received TiO_2 nanoparticle films were sensitized with 0.5 mM ruthenium-based N3 dye solution for 24 h. The samples were then rinsed with ethanol to remove excess dye on the surface and dried at room temperature.

2.2. Solar Cell Assembly

A small piece of weigh paper was placed at each edge of the sensitized TiO_2 nanoparticle film and a Pt-coated silicon substrate as the counter electrode was placed on the top. The device was held in place with two clips on opposite ends. The liquid electrolyte used in this work was composed of 0.6 M tetrabutylammonium iodide, 0.1 M lithium iodide, 0.1 M iodine and 0.5 M 4-tert-butylpyridine in acetonitrile.

2.3. Amount of Dye Adsorption

To measure the adsorbed N3 dye amount on the TiO_2 nanoparticle films, the dye was desorbed by immersing dye-sensitized TiO_2 nanoparticle film in a 0.1 M NaOH solution in water and ethanol (1:1, v/v) for 24 h.

2.4. Characterization Techniques

Thermogravimetric analysis (TGA 7, Perkin-Elmer) was used to investigate the thermal behavior of the dried film as a function of the annealing temperature. X-ray Diffraction (XRD, Philips PW 1830 Diffractometer) was used to verify the phase and particle size of the TiO_2 nanoparticle films. An ultraviolet-visible-near infrared spectrophotometer (UV-VIS-NIR, Perkin Elmer Lambda 900) was employed to measure the dye concentration of the desorbed-dye solution. Scanning electron microscopy (SEM, JEOL JSM-7000) was used to study the morphology of the annealed TiO_2 nanoparticle films. Brunauer Emmett Teller (BET, Quantachrome NOVA 4200e) was used to analyze the surface area of the TiO_2 nanoparticle films. Photovoltaic properties of each solar cell were characterized using simulated AM 1.5 sunlight illumination with an output power of 100 mW/cm^2. An Ultraviolet Solar Simulator (Model 16S, Solar Light Co., Philadelphia, PA) with a 200 W Xenon Lamp Power Supply (Model XPS 200, Solar Light Co., Philadelphia, PA) was used as the light source, and a Semiconductor Parameter Analyzer (4155A, Hewlett-Packard, Japan) was used to measure the current and voltage. The electrochemical impedance spectroscopy (EIS) was carried out through the Solartron 1287A coupling with the Solartron 1260 FRA/impedance analyzer to investigate electronic and ionic processes in DSCs based on TiO_2 nanoparticle films.

3. RESULTS AND DISCUSSION

3.1. Thermal Analysis

Figure 1 shows the thermal behavior of the TiO_2 paste composed of TiO_2 nanoparticles and the organic binder dried at 150 °C for 30 min. The thermogram presents negligible weight loss up to 190 °C. However, a large weight loss of about 23% is observed at temperatures between 190 °C and 350 °C, indicating the oxidation of the organic compounds including α-terpineol and ethyl cellulose.[30, 31] At temperatures higher than 350 °C, no further weight loss is observed, indicating the complete removal of organic residues and clean surface of the TiO_2 nanoparticles is obtained.

3.2. XRD Patterns of Annealed TiO_2 Nanoparticle Films

The XRD patterns of TiO_2 nanoparticle films on FTO substrates annealed at different temperatures, 300 °C, 450 °C and 600 °C, are shown in Figure 2. The patterns for all three temperatures show an anatase TiO_2 phase structure (JCPDS card no. 21-1272) and no existence of the rutile phase structure. It indicates that the annealing process of the film did not cause any detectable change in phase

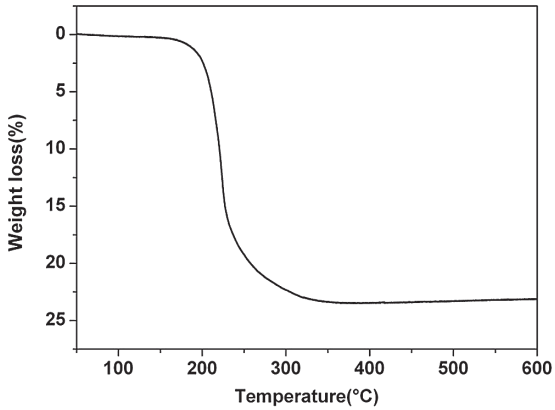

Fig. 1. TGA curve of the dried TiO_2 paste tested in air from room temperature to 600 °C with a heating rate of 3 °C min^{-1}.

structure of original TiO_2 nanoparticles, even at the low (300 °C) and high temperature (600 °C). The transition from anatase to rutile phase usually occurs at high temperature over 600 °C.[32–34] It is helpful to study the properties of the film by changing the annealing temperature, which not affects the nanoparticle itself, for better understanding the relationship between film quality and solar cell performance. The TiO_2 nanocrystallites are not oriented and a slight shift of the peaks due to the presence of the FTO peaks. Using Scherrer's equation, it was found that the crystallite size of the annealed nanoparticles films exhibited a growth from 16 to 22 nm by raising the annealing temperature from 300 °C to 450 °C, and maintained the same size at 600 °C.

3.3. Photovoltaic Performance of DSCs with TiO_2 Nanoparticle Films

The performances of the dye-sensitized solar cells composed of the TiO_2 nanoparticle photoelectrodes are investigated relative to different annealing temperatures from 300 °C up to 600 °C. The open-circuit voltage (V_{oc}), short-circuit current density (J_{sc}), fill factor (FF), and power conversion efficiency (PCE, η) of the DSCs are summarized in Table I. Figure 3 also plotted the DSC performance parameters (V_{oc}, J_{sc}, FF, and PCE) as a function of the annealing temperatures. It is observed that the performance of the DSCs improved significantly by raising the annealing temperature from 300 °C to 350 °C. The DSCs with the TiO_2 nanoparticle photoelectrode annealed at 300 °C reached a PCE of 2.28%, whereas that with the TiO_2 nanoparticle photoelectrode annealed at 350 °C achieved an efficiency of 5.08%. The remarkable improvement (~122%) in power conversion efficiency was the result of the increased J_{sc} and V_{oc}, while FF showed a little decrease. The increase in the annealing temperature from 300 °C to 350 °C resulted in getting rid of the remnant of the organic binder, allowing more dye molecules to attach on the surface of the mesoporous TiO_2 photoelectrode to generate more photocurrent. And the decrease of surface defects by increasing the annealing temperature reduced the recombination of the photo-excited carriers, leading to the improvement of V_{oc}. Figure 3(a) shows a slight change in the performance of DSCs annealed between 350 °C and 600 °C. It is interesting to note that annealing the samples at high temperature more than 350 °C did not add much contribution to the overall performance of the solar cells. Although a slight increase of the photocurrent is observed at $T > 350$ °C probably due to better contact between the nanoparticles, in the opposite a slight reduction of the fill factor make the variation of overall efficiency within 5%, as shown in Figure 3(b). This study revealed that it is not necessary to anneal the well-crystallized TiO_2 nanoparticle photoelectrodes at temperatures much higher than 350 °C, though 450 °C and 500 °C have been common used in literatures as the promising temperature to entirely transform to anatase phase.[1, 29, 35, 36] Electrical conductivities of FTO and ITO substrates may decrease by high temperature annealing, which could affect the power conversion efficiency. Besides, low temperature annealing may save energy and cost for manufacturing.

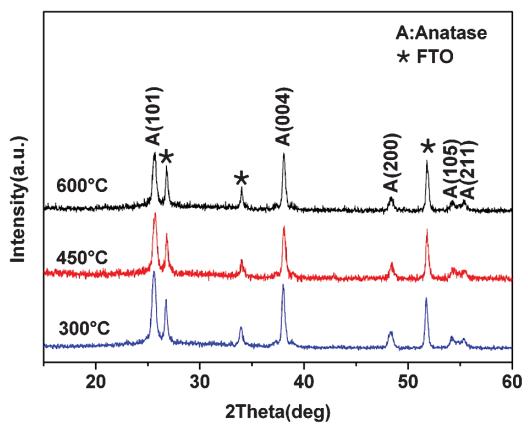

Fig. 2. XRD patterns of TiO_2 nanoparticle films on FTO substrates calcined at different annealing temperatures: 300 °C, 450 °C and 600 °C.

Table I. Summary of open-circuit voltage (V_{oc}), short-circuit current density (J_{sc}), fill factor (FF), and power conversion efficiency (PCE, η) relative to the DSCs based on TiO_2 nanoparticles annealed at different temperatures.

Sample	V_{oc} (V, <±0.01 V)	J_{sc} (mA/cm^2)	FF (<±0.01)	η(%)
300 °C	0.657	5.53±0.15	0.628	2.28±0.06
350 °C	0.755	11.48±0.08	0.587	5.08±0.03
400 °C	0.768	11.92±0.11	0.566	5.17±0.13
450 °C	0.760	11.94±0.29	0.564	5.11±0.01
500 °C	0.759	12.42±0.14	0.552	5.20±0.04
550 °C	0.759	12.68±0.13	0.546	5.25±0.06
600 °C	0.768	11.71±0.43	0.555	4.99±0.10

ARTICLE

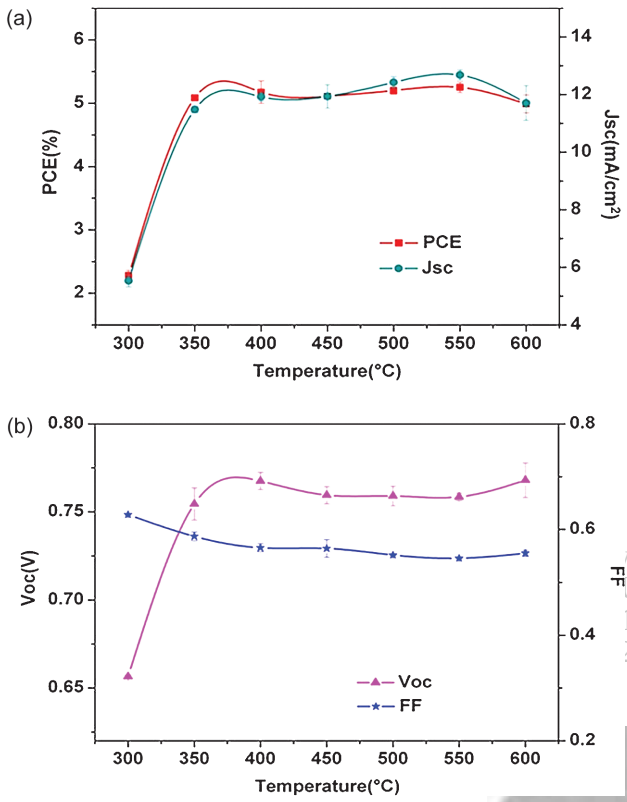

Fig. 3. (a) power conversion efficiency (PCE) and short-circuit current density (J_{sc}), and (b) open-circuit voltage (V_{oc}) and fill factor (FF) are plotted as a function of annealing temperatures.

3.4. Dye Adsorption Behavior of Annealed TiO_2 Nanoparticle Films

The surface area and the adsorbed dye amounts per unit area of the TiO_2 nanoparticle films annealed at different temperatures were investigated. Figure 4 shows the variation of the surface area of the TiO_2 nanoparticle films and the dye detached from each sensitized film as a function of annealing temperature. The surface area and pore volume of TiO_2 nanoparticle films annealed at different temperatures are listed in Table II. It should be pointed out that the surface area of TiO_2 nanoparticle film annealed at 300 °C is not measured since organic residue (carbon) was not removed completely, as the annealed films appear grey. The surface area of TiO_2 nanoparticle film decreases from 126 m^2/g to 109 m^2/g by increasing the annealing temperature from 350 °C to 400 °C, caused by the increase in the crystal size of TiO_2 nanoparticles from 16 nm to 22 nm, calculated from the XRD patterns. With a higher annealing temperature, the surface area decreases further and the pore volume shows a similar trend, suggesting that densification via grain boundary diffusion in addition to sintering through surface diffusion occurred, though the annealing temperature is relatively low for typical ceramic processing. Densification occurred at such low temperature may

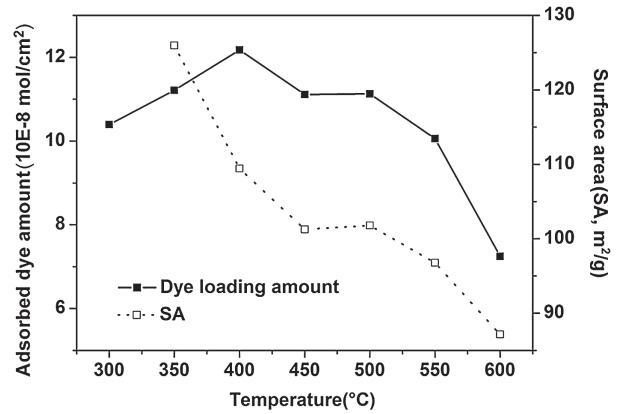

Fig. 4. Comparison of the surface area per unit weight and the amount of dye adsorbed per unit area of the TiO_2 photoelectrodes annealed at the different temperatures. The lines just serve as a visual guide.

be well attributable to large surface energy of nanostructured TiO_2 particles.[37]

It was found that the amount of dye adsorbed per unit area of films exhibited an increase by rising the annealing temperature from 300 °C to 350 °C. The removal of the organic binder released some of the surface area of nanoparticles which benefits for the dye loading. However, by further increasing the annealing temperature to 400 °C, the adsorbed dye amount still shows an increase in spite of the decrease in surface area allowable for dye adsorption. The similar results had been reported in literature,[29] probably because the films consisting of larger particles had greater effective surface area for photon adsorption and electron–hole pair generation. In addition, the remove of the organic binder may cause the oxygen vacancies on the surface of TiO_2 nanoparticles, which may be not favorable for dye adsorption. It was expected that the amount of dye adsorbed per unit area of photoelectrodes dropped gradually by increasing the annealing temperature from 400 °C to 600 °C, corresponding to the decreasing specific surface area of TiO_2 nanoparticle films. The reduction of adsorbed dye amount would decrease the generation of electron–hole pairs, resulting in a decrease in the short-circuit current density as well as power conversion efficiency, when other parameters or properties remain unchanged.

Table II. BET results for the TiO_2 photoelectrodes annealed at the different temperatures.

Sample	Surface area (m^2g^{-1})	Pore volume (ccg^{-1})
350 °C	125.96	0.344
400 °C	109.46	0.304
450 °C	101.25	0.302
500 °C	101.76	0.294
550 °C	96.78	0.260
600 °C	87.16	0.240

3.5. Morphology of Annealed TiO_2 Nanoparticle Films

Figure 5 shows SEM images of the surface morphologies of TiO_2 nanoparticle films sintered at different temperatures. Figures 5(a)–(c) show the low magnification SEM images of the film morphologies of TiO_2 nanoparticle films annealed at 350 °C, 450 °C and 600 °C, respectively. The film sintered at 450 °C showed a much rougher surface with more pores visible, as shown in Figure 5(b), than that of the film annealed at 350 °C shown in Figure 5(a). Figure 5(c) shows the well connected network due to the neck growth between nanoparticles. Figures 5(d)–(f) show the high magnification SEM images of the TiO_2 films annealed at 350 °C, 450 °C and 600 °C, respectively. The sample annealed at higher temperature shows more sintering of the nanoparticles, which merged together to form the neck between nanoparticles with better contact between the adjacent nanoparticles for efficient electron transfer.

3.6. Electron Transport Properties of DSCs with TiO_2 Nanoparticle Films

EIS spectra of dye-sensitized solar cells with the TiO_2 photoelectrodes annealed at different temperatures were measured at the open circuit condition and presented together with an equivalent circuit in Figure 6. The large arc on the right side in Figure 6(b), or the low-frequency semicircle corresponds to charge-transfer resistance (charge recombination resistance, R_{ct}) between TiO_2 and oxidized species in electrolyte. Figure 6(c) shows the fitted value of R_{ct} as a function of the annealing temperature. The EIS spectrum of the sample annealed at 300 °C exhibits different behavior, as compared with samples annealed at higher temperatures. An appreciable shift of the peak in the low frequency semicircle (shown in Fig. 6(b)), and a sharp increase of R_{ct} from 92 to 133 Ω when the annealing temperature increased from 300 °C to 350 °C (shown in Fig. 6(c)). According to Kern's model[38] the charge recombination can take place not only between the electrons in the conduction band and the oxidized species in electrolyte, but also between the electrons at surface trapping states and oxidized species. The surface states of nanoparticles are physically located either at the surface or within a tunneling distance.[39] In general, the surface states can trap electrons rapidly and release very slowly. The trapping is about 1,000 times faster than de-trapping, which makes the density of trapped electrons at the surface states is many orders of magnitude higher than the density of electrons in the conduction band.[38, 40] Thus, the recombination between the free conduction band electrons and the oxidized species of the electrolyte can be neglected in comparison to the recombination between the trapped electrons at the surface states and the oxidized species.[38] At low temperature 300 °C, incomplete pyrolysis of organics introduces impurities including carbon as discussed earlier section in this paper, and surface defects, affecting directly on the charge recombination, thus influencing both photocurrent and photovoltage of the DSCs, in a good

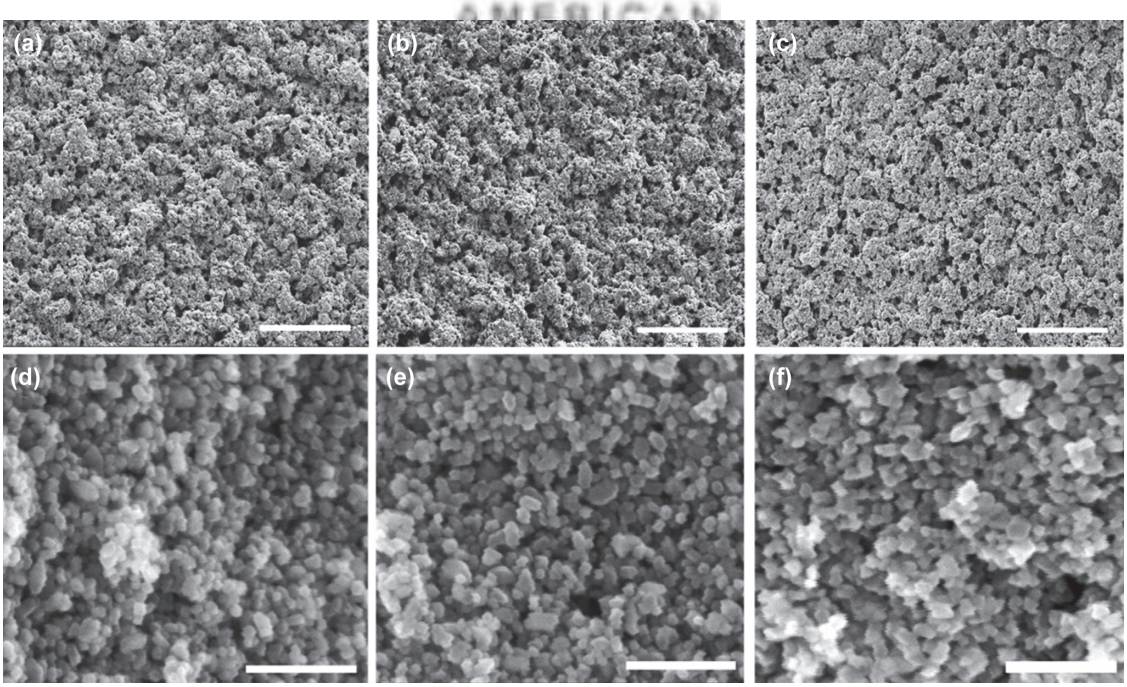

Fig. 5. SEM micrograph of the surface of TiO_2 layers annealed at (a) and (d) 350 °C, (b) and (e) 450°C, (c) and (f) 600°C. Scale bar in (a), (b) and (c) is 100 μm, in (d), e) and (f) is 200 nm.

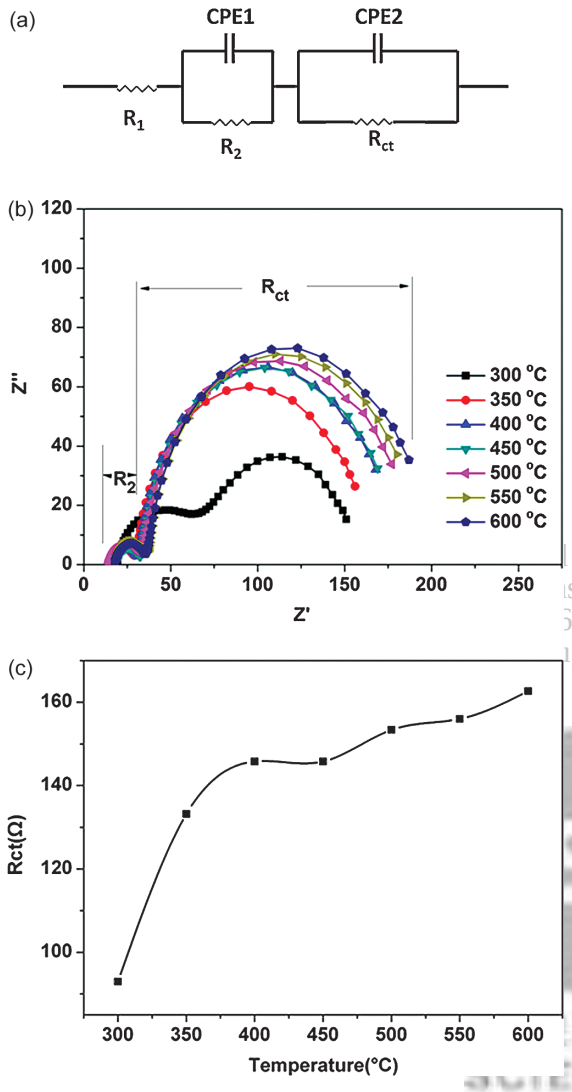

Fig. 6. (a) The fitted equivalent circuit, (b) EIS spectroscopy for the DSSCs made of different TiO_2 photoanodes annealed at different temperature, (c) charge-transfer resistance as a function of annealing temperatures.

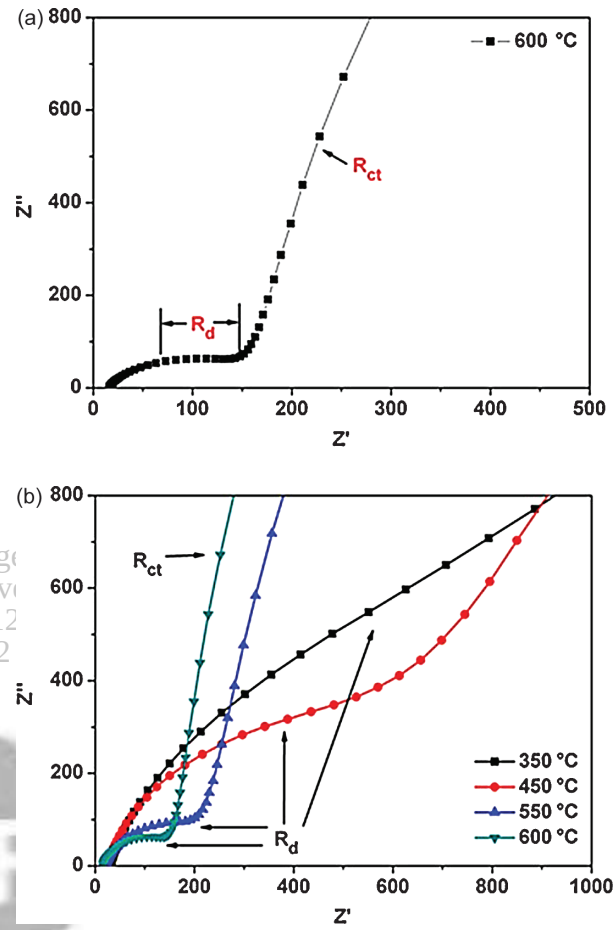

Fig. 7. (a) EIS spectra of the TiO_2 films annealed at 600 °C, measured at bias voltage −0.5 V, in which a diffusion resistance (R_d) and a charge transport resistance (R_{ct}) were pointed out, (b) Nyquist plot of R_d as a function of annealing temperatures, measured at bias voltage −0.5 V.

agreement with the results listed in Table I. By further increasing the annealing temperature, a gradual increase of R_{ct} is observed in Figure 6(c), which is attributed to further sintering and densification with reduced surface area and the surface states, leading to the suppression of charge recombination between the trapped electrons at the surface states and the oxidized species. However, according to our results shown in Figure 3(b), the change of R_{ct} by increasing the annealing temperatures did not affect the V_{oc}, which is consistent with that reported in ref 18 but still need further explanations.

Fabregat et al.[41] proposed that the low frequency semicircle is fitted to R_{ct} connected with the electron diffusion resistance (R_d) in TiO_2 photoelectrodes in series. However, in practice it is difficult to separate R_d from R_{ct} at the open circuit condition since R_d is overlapped at the position where transition from the first semicircle to second semicircle occurs. With a decrease of the applied bias voltage, R_d would be represented as Warburg-like diffusion behavior. To investigate the effects of annealing temperature on R_d, EIS measurement was carried out at a bias voltage of −0.5 V. Figure 7(a) shows the diffusion resistance as the straight line appeared before the second semicircle in Nyquist plot of photoelectrode annealed at 600 °C, measured at bias voltage −0.5 V. Figure 7(b) compares the electron diffusion resistances of photoelectrodes annealed at different temperatures. A gradual reduction of the electron diffusion resistance is observed with an increasing annealing temperature from 350 °C to 600 °C, which can be simply ascribed to the growth of neck between adjacent TiO_2 nanoparticles in photoelectrodes. The reduced diffusion resistance in the TiO_2 photoanodes favors efficient electron transport and collection which may result in the reduced chance of charge recombination and the enhancement of short-circuit current density as well as power conversion efficiency.

4. CONCLUSIONS

This work revealed significant influences of annealing temperature on the microstructure, dye-adsorption, charge transport, and power conversion efficiency of well-crystallized TiO_2 nanoparticle DSCs. An annealing at temperature lower than 350 °C leads to incomplete removal of organic compounds and introduces carbon impurities and surface defects, which hinder the dye adsorption and promote charge recombination, resulting in both low photocurrent density and low open circuit voltage of the DSCs. Increased annealing temperature would reduce the specific surface area as well as the amount of adsorbed dye molecules through partial sintering, leading to less photons captured. However, the partial sintering results in the better contact between the adjacent nanoparticles which benefits for the efficient electron transport and collection. All the competing changes combined, the DSCs would achieve a relative constant PCE of $5.1 \pm 0.2\%$ with a negligible deviation for the samples annealed at temperatures higher than 350 °C, which allows saving the manufacturing energy and cost. For further enhancement of solar cell performance, the improved charge transport properties should not be achieved at the expense of specific surface area.

Acknowledgment: JTX gratefully acknowledges the fellowship from China Scholarship Council. Professor Naji Al Dahoudi would like to acknowledge Fulbright Scholarship. And this work has been supported in part by National Natural Science Foundation of China (21173042), Natural Science Foundation of Jiangsu Province (BK2011589), the US Department of Energy, Office of Basic Energy Sciences, Division of Materials and Engineering under Award No. DE-FG02-07ER46467 (Q.F.Z.) on the microstructure characterization and some power conversion efficiency measurements, National Science Foundation (DMR-1035196), Boeing-Steiner Endowment, University of Washington TGIF grant and Intel Corporation.

References and Notes

1. B. Oregan and M. Grätzel, *Nature* 353, 737 **(1991)**.
2. M. Grätzel, *Nature* 414, 338 **(2001)**.
3. Q. F. Zhang, C. S. Dandeneau, X. Y. Zhou, and G. Z. Cao, *Adv. Mater.* 21, 4087 **(2009)**.
4. A. Shah, P. Torres, R. Tscharner, N. Wyrsch, and H. Keppner, *Science* 285, 692 **(1999)**.
5. M. Grätzel, *Philos. Trans. R. Soc. London, Ser. A* 365, 993 **(2007)**.
6. A. Goetzberger, J. Luther, and G. Willeke, *Sol. Energy Mater. Sol. Cells* 74, 1 **(2002)**.
7. Q. F. Zhang and G. Z. Cao, *Nano Today* 6, 91 **(2011)**.
8. A. B. F. Martinson, T. W. Hamann, M. J. Pellin, and J. T. Hupp, *Chem. Eur. J.* 14, 4458 **(2008)**.
9. L. M. Peter, *J. Phys. Chem. C* 111, 6601 **(2007)**.
10. T. W. Hamann and J. W. Ondersma, *Energ. Environ. Sci.* 4, 370 **(2011)**.
11. J. Bisquert, *J. Phys. Chem. B* 106, 325 **(2002)**.
12. N. G. Park, J. van de Lagemaat, and A. J. Frank, *J. Phys. Chem. B* 104, 8989 **(2000)**.
13. M. K. Nazeeruddin, F. De Angelis, S. Fantacci, A. Selloni, G. Viscardi, P. Liska, S. Ito, T. Bessho, and M. Grätzel, *J. Am. Chem. Soc.* 127, 16835 **(2005)**.
14. K. M. Lee, V. Suryanarayanan, and K. C. Ho, *Sol. Energy Mater. Sol. Cells* 90, 2398 **(2006)**.
15. P. M. Sommeling, B. C. O'Regan, R. R. Haswell, H. J. P. Smit, N. J. Bakker, J. J. T. Smits, J. M. Kroon, and J. A. M. van Roosmalen, *J. Phys. Chem. B* 110, 19191 **(2006)**.
16. C. Longo, A. F. Nogueira, M. A. De Paoli, and H. Cachet, *J. Phys. Chem. B* 106, 5925 **(2002)**.
17. F. Pichot, J. R. Pitts, and B. A. Gregg, *Langmuir* 16, 5626 **(2000)**.
18. S. Nakade, M. Matsuda, S. Kambe, Y. Saito, T. Kitamura, T. Sakata, Y. Wada, H. Mori, and S. Yanagida, *J. Phys. Chem. B* 106, 10004 **(2002)**.
19. K. M. Lee, V. Suryanarayanan, and K. C. Ho, *Sol. Energy Mater. Sol. Cells* 91, 1416 **(2007)**.
20. G. Kantonis, T. Stergiopoulos, A. P. Katsoulidis, P. J. Pomonis, and P. Falaras, *J. Photochem. Photobiol. A* 217, 236 **(2011)**.
21. D. Zhao, T. Y. Peng, L. L. Lu, P. Cai, P. Jiang, and Z. Q. Bian, *J. Phys. Chem. C* 112, 8486 **(2008)**.
22. M. C. Kao, H. Z. Chen, and S. L. Young, *Thin Solid Films* 519, 3268 **(2011)**.
23. M. C. Kao, H. Z. Chen, S. L. Young, C. Y. Kung, C. C. Lin, and J. Z. Lai, *J. Supercond Nov. Magn.* 23, 897 **(2010)**.
24. K. Zhu, N. R. Neale, A. F. Halverson, J. Y. Kim, A. J. Frank, *J. Phys. Chem. C* 114, 13433 **(2010)**.
25. K. Park, J. Xi, Q. Zhang, and G. Cao, *J. Phys. Chem. C* 115, 20992 **(2011)**.
26. P. J. Cameron and L. M. Peter, *J. Phys. Chem. B* 109, 7392 **(2005)**.
27. J. Bisquert, D. Cahen, G. Hodes, S. Ruhle, and A. Zaban, *J. Phys. Chem. B* 108, 8106 **(2004)**.
28. E. Bertran, C. Corbella, M. Vives, A. Pinyol, C. Person, and I. Porqueras, *Solid State Ionics* 165, 139 **(2003)**.
29. T. P. Chou, Q. F. Zhang, B. Russo, G. E. Fryxell, and G. Z. Cao, *J. Phys. Chem. C* 111, 6296 **(2007)**.
30. M. Nedelcu, S. Guldin, M. C. Orilall, J. Lee, S. Huttner, E. J. W. Crossland, S. C. Warren, C. Ducati, P. R. Laity, D. Eder, U. Wiesner, U. Steiner, and H. J. Snaith, *J. Mater. Chem.* 20, 1261 **(2010)**.
31. R. Mori, T. Ueta, K. Sakai, Y. Niida, Y. Koshiba, L. Lei, K. Nakamae, and Y. Ueda, *J. Mater. Sci.* 46, 1341 **(2011)**.
32. Y. Djaoued, S. Badilescu, P. V. Ashrit, D. Bersani, P. P. Lottici, and J. Robichaud, *J. Sol–Gel Sci. Technol.* 24, 255 **(2002)**.
33. D. J. Won, C. H. Wang, H. K. Jang, and D. J. Choi, *Appl. Phys. A* 73, 595 **(2001)**.
34. Y. H. Tseng, H. Y. Lin, C. S. Kuo, Y. Y. Li, and C. P. Huang, *React. Kinet. Catal. Lett.* 89, 63 **(2006)**.
35. P. Wang, S. M. Zakeeruddin, J. E. Moser, M. K. Nazeeruddin, T. Sekiguchi, and M. Grätzel, *Nature Materials* 2, 402 **(2003)**.
36. M. Grätzel, *J. Sol–Gel Sci. Technol.* 22, 7 **(2001)**.
37. K. N. P. Kumar, K. Keizer, A. J. Burggraaf, T. Okubo, H. Nagamoto, and S. Morooka, *Nature* 358, 48 **(1992)**.
38. R. Kern, R. Sastrawan, J. Ferber, R. Stangl, and J. Luther, *Electrochim. Acta* 47, 4213 **(2002)**.
39. J. Bisquert, A. Zaban, M. Greenshtein, and I. Mora-Sero, *J. Am. Chem. Soc.* 126, 13550 **(2004)**.
40. L. M. Peter, *Phys. Chem. Chem. Phys.* 9, 2630 **(2007)**.
41. F. Fabregat-Santiago, J. Garcia-Canadas, E. Palomares, J. N. Clifford, S. A. Haque, J. R. Durrant, G. Garcia-Belmonte, and J. Bisquert, *J. Appl. Phys.* 96, 6903 **(2004)**.